Synthesis mechanism of different morphological SiC and its electromagnetic absorption performance

Jinyan Wang, Jiaqi Tao, Jintang Zhou, Harm Van Zalinge, Zhengjun Yao, Li Yang

PII: S1044-5803(23)00687-3

DOI: https://doi.org/10.1016/j.matchar.2023.113328

Reference: MTL 113328

To appear in: *Materials Characterization*

Received date: 19 July 2023

Revised date: 8 September 2023

Accepted date: 14 September 2023

Please cite this article as: J. Wang, J. Tao, J. Zhou, et al., Synthesis mechanism of different morphological SiC and its electromagnetic absorption performance, *Materials Characterization* (2023), https://doi.org/10.1016/j.matchar.2023.113328

Synthesis mechanism of different morphological SiC and its electromagnetic absorption performance

Jinyan Wang[a,b,c], Jiaqi Tao[b], Jintang Zhou[b,*], Harm Van Zalinge[a], Zhengjun Yao[b,*], Li Yang[c,**]

[a] Department of Electrical Engineering and Electronics, University of Liverpool, Liverpool, L69 3GJ, United Kingdom

[b] College of Materials Science and Technology, Nanjing University of Aeronautics and Astronautics, Nanjing, 211100, Jiangsu, People's Republic of China

[c] Department of Chemistry, Xi'an Jiaotong-Liverpool University, Suzhou, 215123, Jiangsu, People's Republic of China

[*] Corresponding author. College of Materials Science and Technology, Nanjing University of Aeronautics and Astronautics, Nanjing, 211100, Jiangsu, People's Republic of China.

[**] Corresponding author. Department of Chemistry, Xi'an Jiaotong-Liverpool University, Suzhou, 215123, Jiangsu, People's Republic of China

Email: yaozj1921@126.com (Z. Yao), imzjt@126.com (J. Zhou), li.yang@xjtlu.edu.cn (L. Yang)

Abstract

This article presents a facile synthesis of different morphological silicon carbides (SiC) absorbers by adjusting the weight ratio of carbon spheres to waste glass powder. With the decreased proportion of waste glass powder, the diffusion rate of SiO vapour decreases, which is lower than the deposition rate, leading to the morphology change from fluffy spheres to nanofibers. The electromagnetic wave (EMW) absorbing

results show that the fluffy spherical SiC possesses the optimal EMW absorption performance with an effective absorption bandwidth 4.81 GHz at 1.6 mm, mainly due to stacking faults-induced polarisation loss and conductive loss. By comparison, the EMW absorbing ability of SiC obtained through wasted glass powder is better than the normal SiC prepared through commercial SiO_2. Thus, the waste glass has shown great promise as silicon resources to prepare high-performance SiC absorbers.

Keywords: Electromagnetic absorbing performance, SiC absorber, synthesis mechanism, stacking faults, waste glass powder.

1 Introduction

Electromagnetic wave (EMW) pollution has been overgrowing with the development of technology and has now become the fourth pollution after air, water and noise pollution [1]. Excessive EMW radiation can expose living organisms to potential health risks. Shi et al. [2] discovered that specific electromagnetic radiation in wireless signal ranges increases wakefulness in mice. Gandhi et al. [3] found that static electromagnetic fields significantly affect sleep onset and duration through the thermal model of human body analysis. Thus, various EMW absorbers that can effectively absorb EMWs have been developed to solve the problems mentioned above [4-8].

Silicon carbide (SiC) is a dielectric absorber [9] and can be applied in extreme working circumstances due to its high-temperature oxidation resistance, high strength, low density, and good chemically inert [10, 11]. It has been reported that SiC with different morphology shows significantly different wave absorber properties. A series of experiments have been carried out to prepare SiC with different morphology. For example, Wu et al. [12] used bamboo pulp paper as a carbon source and commercial Si and SiO_2 as a silicon source to prepare a bamboo-shaped SiC whisker absorber.

The effective absorption bandwidth (EAB) is 3.4 GHz at a thickness of 2.5 mm. Xiao et al. [13] adopted carbon fibre as a carbon source and commercial SiO_2 as a silicon source to synthesise fabric SiC composite absorbers. The EAB is 5 GHz at 2 mm. Liu et al. [14] prepared porous interconnected SiC through apple fruit. The porous interconnected morphology of apple fruit was perserved. The EAB can reach 4 GHz with a 4.0-5.0 mm sample thickness. All these previous work confirm that SiC has a good shape memory on the carbon sources and is a good EMW absorber. Therefore, efforts to develop well-controlled morphology SiC have been a great impetus to the field of EMW radiation. Until now, the research on morphology with synthesis mechanisms is rarely studied.

The traditional way to prepare SiC is through the high-temperature reaction of silicon and carbon resources, which can be explained as a vapour-solid (VS) or vapour-solid-liquid (VSL) mechanism. For VS reaction, enough SiO vapour can be generated at 1200 ℃, which can further react with solid carbon sources and keep the shape of carbon sources. For example, Liang et al. [15] synthesized an eggplant-derived SiC absorber, and the shape of the products is consistent well with eggplant through VS reaction. For VSL reaction, some other substances can form a molten or liquid solution at high temperatures and promote the reaction between silicon and carbon sources. Liu et al. [16] synthesised a hollow SiC@C absorber through the VSL mechanism between resorcinol formaldehyde resin and self-prepared SiO_2 by adding a metal catalyst, which can become the molten solution at high temperature and serve as the site for forming SiC. However, the synthesis mechanism of the SiC absorber and the relationship between morphology and reaction was relatively vague in those early studies.

In this work, SiC absorbers with different morphologies were prepared by adjusting

the proportion of waste glass powder. The change in the morphology is due to the competitive process where diffusion and deposition occur simultaneously [17]. When the ratio of carbon spheres to glass powder was 1 to 1, there were enough silicon resources to ensure that the diffusion rate was higher than the deposition rate, resulting in fluffy, porous, spherical SiC, which had an excellent EMW absorption performance. The minimum reflection loss (RL_{min}) value of SiC is -48.92 dB at 8.96 GHz. The EAB of the product reaches 4.81 GHz at 1.6 mm. In contrast, the normal SiC were synthesised through commercial SiO_2, and its EMW absorbing performance was tested. The result shows that its EMW absorbing capacity is slightly worse than SiC prepared by the waste glass. This work analysed the formation mechanism of different morphological SiC absorbers and presents a new method to recycle waste glass.

2 Experimental sections

2.1 Materials

A ball-milling machine milled waste glass, and X-ray fluorescence tested the main ingredients with the components of SiO_2 (71.55 wt%), Na_2O (13.2 wt%), Al_2O_3 (5.96 wt%), and CaO (3.37 wt%). Tetraethyl orthosilicate (TEOS), ammonium hydroxide solution ($NH_3 \cdot H_2O$, 25-28 wt%), ethanol absolute (EtOH), sucrose, silicon powder (Si, 3000 mesh), sodium polyacrylate (PAAS, average Mw 4000K-5000K), hydrofluoric acid (HF，40 wt%). All materials, including distilled water, were purchased from Macklin and used without further purification.

2.2 Preparation of monodisperse carbon sphere templates

The monodisperse carbon sphere templates were synthesised through a hydrothermal reaction. 2 g sucrose was dissolved in 40 ml of distilled water, and 30 mg PAAS was added. After violently whisking for 60 minutes, the solution was

shifted from the beaker to 50 ml Teflon and heated to 190 ℃ for 5 hours. The monodisperse carbon sphere templates were obtained after centrifugation and dried at 60 ℃ overnight.

2.3 Preparation of SiC with tunable morphology

The brown carbon spheres were mixed with waste glass powder according to different ratios (the weight ratio of carbon spheres to glass powder was 1:1, 2:1 and 4:1, respectively). Then, the mixture was put into a corundum crucible in a tube furnace under the protection of an argon atmosphere. The furnace temperature was controlled with a program of heating of 550 °C at 2 ℃·min^{-1}, holding at 550 ℃ for 3 hours, further heating to 1400 ℃ at 2 ℃·min^{-1}, respectively, holding for 8 hours and then cooling to room temperature at 5 ℃·min^{-1}. Subsequently, excess silicon resources and impurities were removed with HF overnight. SiC with different morphologies were obtained by eliminating the excessive carbon in a muffle furnace at 650 ℃ for 3 hours. The final samples were named G-1-1, G-2-1, and G-4-1, respectively. In contrast, the same amount of commercial SiO_2 was used to prepare normal SiC and labelled C-1-1, C-2-1, and C-4-1, respectively. (Note: G represents glass powder, and C represents commercial silicon. The first number represents the amount of carbon spheres, and the second represents the amount of silicon sources.)

2.4 Characterisation

The ingredients of the waste glass powder were tested by X-ray fluorescence (XRF). The crystalline phases and phase purity of the products were tested by an X-ray diffraction (XRD), operated at 40 kV and 40 mA and the 2 theta from 10 ˚ to 80 ˚ with the speed of 5 ˚·min^{-1}. Raman spectra were recorded on a Xplo RA Raman spectrometer with a spectral range from 500 cm^{-1} to 1100 cm^{-1} using a laser of 532 nm. The microstructure of the products was observed through field emission scanning

electron microscope (FESEM). The hollow morphology was tested on a transmission electron microscope (TEM). The thermal stability of the products was studied on a thermal gravimetric analyser (TGA) from 30 ℃ to 800 ℃ in an environment in which the air was untreated with a heating rate of 10 ℃·min^{-1}. The specific surface area and pore size of each sample were tested by a Nitrogen adsorption-desorption analyser (BET). The band gap characteristics of SiC are measured through an Ultraviolet spectrophotometer (UV-Vis), and the wavelength ranges from 200 nm to 800 nm. The electromagnetic wave absorption performance was tested by a vector network analyser (VNA) between 2 GHz and 18 GHz using a circular ring obtained by mixing with wax with a filling weight ratio of 30 %.

3 Results and discussion

Fig.1 (a) schematically illustrates the synthesis process and how the weight ratio of glass powder experimentally determines the morphology of SiC. First, monodisperse carbon sphere templates were prepared through a hydrothermal reaction of sucrose at 190 ℃. It is worth mentioning that surfactant PAAS is crucial to synthesising monodisperse carbon sphere templates (Fig.1 d and e). PAAS has high molecular weight and produces steric hindrance after absorbing carbon spheres, thus achieving the best dispersion effect [18]. Second, the obtained carbon spheres were mixed with glass powder at a certain concentration and placed into a tube furnace at 1400 ℃. After a high-temperature reaction, the monodisperse carbon sphere templates can be maintained (Fig.1 f). Different morphology of pure SiC can be obtained after the treatment to remove unreacted silicon and carbon. In theory, abundant newly generated atoms shift to lower energy sites by surface diffusion [19]. The waste glass concentration decides the microstructure of SiC between the diffusion and deposition rates of silicon resources. As expected, when the ratio is 1:1, there were sufficient free

silicon resources to diffuse and react with carbon spheres. Thus, the resultant morphology was fluffy flower-like spheres (Fig.1 g). However, the diffusion rate of SiO vapour drops when the concentration of waste glass decreases; at this point, the sphere morphology can become scattered, and the spheres can no longer be maintained (Fig.1 h). As the concentration of glass powder continually declined (4:1), the diffusion rate dropped to a critical level when the deposition rate led to the formation of SiC nanofiber (Fig.1 k).

For the glass powder system, even though the reaction temperature (1400 ℃) did not reach the melt temperature of SiO_2 (1723 ℃), the reaction between SiO_2 and C spheres can occur due to the existence of metallic oxides, which can decrease the temperature of diffusion movements and react as Equation (1) shows. The generated SiO vapour can further react with C templates or CO vapour to generate SiC according to Equations (2) and (3). When the ratio was 1:1, there was sufficient SiO vapour. The diffusion rate is higher than the deposition rate and can form spherical flower-like G-1-1. The diffusion rate declines gradually with the decreasing concentration of silicon resources. As the glass powder concentration dropped to 2:1, the diffusion rate was slightly lower than the deposition rate, and there was insufficient SiO for both Equations (2) and (3). However, Equation (3) is more likely to occur because it requires less energy than Equation (2) [20]. Thus, the sphere morphology cannot be maintained, forming scattered spheres (G-2-1). As the concentration of silicon resources kept falling and reaching 4:1, the deposition rate led to the reaction, and the generated CO_2 reacted with C to form more CO (Equation 4) to speed equation (3). There is almost no reaction occurred on C templates. Thus, the microstructure is nanofibers (G-4-1).

$$SiO_2(s) + C(s) = SiO(g) + CO(g) \quad (1)$$

$$SiO(g) + 2C(s) = SiC(s) + CO(g) \quad (2)$$

$$SiO(g) + 3CO(g) = SiC(s) + 2CO_2(g) \quad (3)$$

$$CO_2(g) + C(s) = 2CO(g) \quad (4)$$

The XRD tests were used to investigate the crystal composition of the samples. The XRD patterns of the products after a high-temperature reaction in the tube furnace showed that the composition of the product changed from silica and silicon carbide to carbon and silicon carbide as the weight ratio of the silicon source decreased (Fig.S1). The XRD patterns (Fig.1 b) of the final products show that the diffraction peaks located at 35.74 ˚, 60.14 ˚, and 71.97 ˚ are the three main peaks of SiC, in a good agreement to (111), (220), and (311) crystal planes of β-SiC (JPCDS PDF#73-1708), respectively. The weak peaks at 41.50 ˚ and 75.71 ˚ correspond to (200) and (222) crystal planes of SiC. A small peak at 33.72 ˚ indicates stacking faults (SF) [21] in β-SiC, which can increase electron energy and polarisation loss. These results demonstrate that we obtained pure SiC with some SF, indicating etching and high-temperature treatment can remove excess silicon and unreacted carbon. The pore properties of the products can be examined by BET measurement. Fig.1 (c) shows the Nitrogen adsorption-desorption curves of each sample and manifests the property of a typical IV isotherm [22-24], indicating pores existed in the prepared SiC. The unique pore morphology improves the matching condition with air and increases air contact surfaces, promoting interfacial polarisation [25]. Fig.S2 shows the specific surface area of each sample. It can be found the particular surface area of SiC gradually decreases with the declining concentration of silicon resources, which is due to the spheres totally transforming into nanofibers. This agrees well with the previous results. The TGA curves (Fig.S3) show different morphological SiC did not lose weight from room temperature to 800 ℃ in air atmosphere, indicating that pure SiC has good

thermal stability.

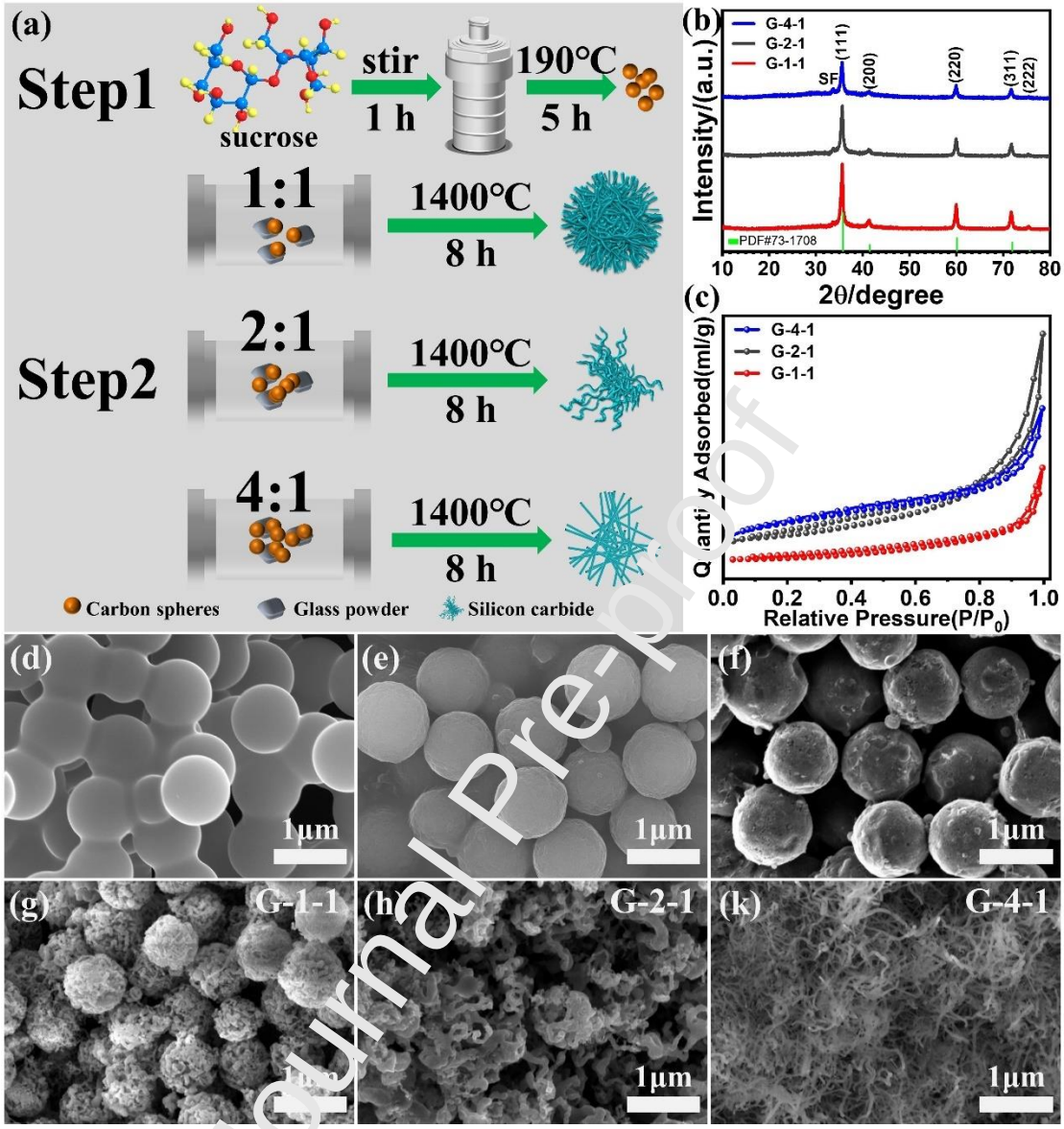

Fig.1 (a) Schematic showing the facile synthesis process of different morphology of SiC in various ratios of carbon spheres to silicon resources. (b) XRD patterns of G-1-1, G-2-1, G-4-1. (c) Nitrogen adsorption-desorption curves of G-1-1, G-2-1, G-4-1. (d) carbon spheres without PAAS. (e) monodisperse carbon spheres with PAAS. (f) SiC@C after high-temperature reaction in the tube furnace. (g-k) pure SiC at different ratios of carbon spheres to waste glass.

TEM tests can further affirm the specific microstructure of SiC in different concentrations of glass powder. As shown in Fig.2 (a-c), the morphology of SiC changes from fluffy spheres to scattered spheres to nanofibers when the ratio ranges

from 1:1 to 2:1 to 4:1. The results fit well with the FESEM test results. Fig.2 (d and d1) are the high-resolution TEM images of G-1-1. Obviously, the surface contains good stacking order, a large number of stepped stripes and a small amount of amorphous phase. A large amount of stepped stripes indicates a high stacking faults (SF) content in SiC, which aligns well with the XRD results. These defects can create a dipole field by unbalanced charge distribution and increase polarisation loss [26]. According to the surface lattice analysis, the distance between crystal planes is 0.251 nm, corresponding to the (111) crystal plane of SiC. The element mapping tests illustrate that C and Si are uniformly distributed at the whole spheres in Fig.2 (e), which also proves the products are pure SiC.

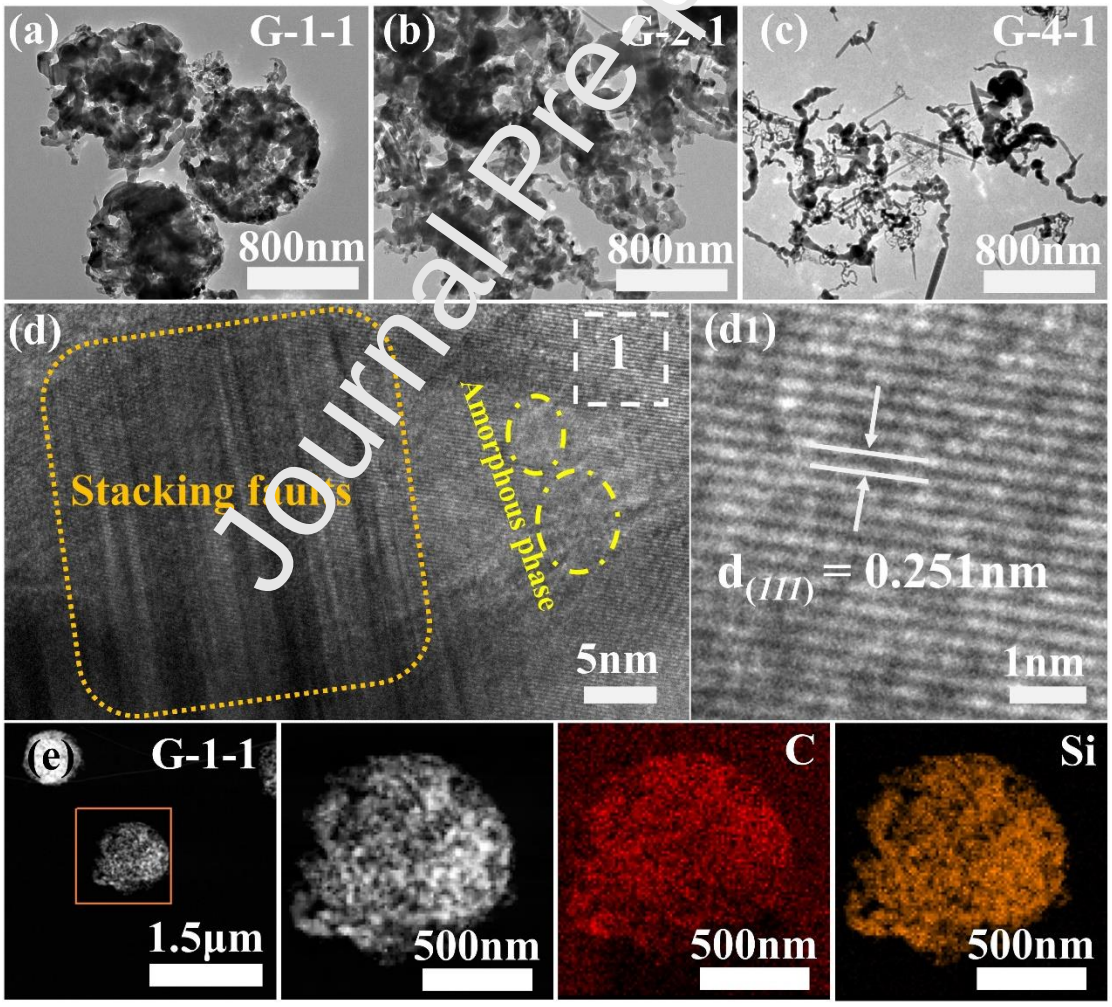

Fig.2 (a-c) Low-resolution TEM images of G-1-1, G-2-1 and G-4-1. (d,d1) High-resolution TEM

images of G-1-1. (e) Element mapping distribution of G-1-1.

To determine the effects of morphology on the EMW absorbing ability, the input impedance is given based on the following equations [27-29]:

$$Z_{in} = Z_0\sqrt{|\mu_\gamma/\varepsilon_\gamma|}\,tanh[j(2\pi fd/c)]\sqrt{\mu_\gamma\varepsilon_\gamma} \quad (5)$$

$$RL = 20\,log_{10}|(Z_{in} - Z_0)/(Z_{in} + Z_0)| \quad (6)$$

where Z_0 means the free space impedance (Z_0=377Ω), Z_{in} is the input impedance of the absorber, *f* is the measured frequency, c is the velocity of EMW in free space, *d* is the thickness of the absorber. From Equation (6), if Z_{in} equals Z_0, then reflection loss (RL) equals 0, which indicates no reflection. However, this ideal impedance-matching condition is very hard to achieve. Therefore, we prepared the EMW absorption material with the input impedance (Z_{in}) close enough to the optimum impedance of the free space. Typically, the RL value of EMW absorbers should be lower than -10 dB, which means that at least 90 % of the EMW energy is absorbed [6, 30].

Fig.3 (a-c) are the 3D graphs of reflection loss of G-1-1, G-2-1 and G-4-1, which can clearly show the trend of reflection loss with frequency and thickness. The EMW absorption ability of G-1-1 and G-2-1 is stronger, while that of G-4-1 is the worst. Fig.3 (d-f) gives intuitive information on the thickness and frequency of each product. The results indicate that the absorbing properties have a relation with the thickness of the products. The biggest RL_{min} value tends to move to a lower frequency by corresponding increases in the thickness, which is caused by the quarter wave principle [31, 32]. When we test the absorption performance, the phase between the incident and reflected waves is 180 ° and counteract, and then the RL_{min} can be obtained. The minimum reflection loss (RL_{min}) values of G-1-1, G-2-1 and G-4-1 are -48.92, -52.5, and -12.64 dB, respectively. To further compare the EMW performance

of different morphology, the reflection loss curves at different thicknesses are shown in Fig.3 (g-k). The EAB values of the samples were 4.81, 3.48, and 1.32 GHz, respectively. The matching thickness were 1.6, 1.9, and 9.5 mm, respectively. Also, the value of RL_{min} under a specific frequency means the match between the medium and free space is nearest. For the thickness of G-1-1 at 2.4 mm, the RL_{min} is -48.92 dB, and the corresponding frequency is 8.96 GHz, showing that electromagnetic waves can maximally enter the product; thus, the sample has the lowest reflection loss value.

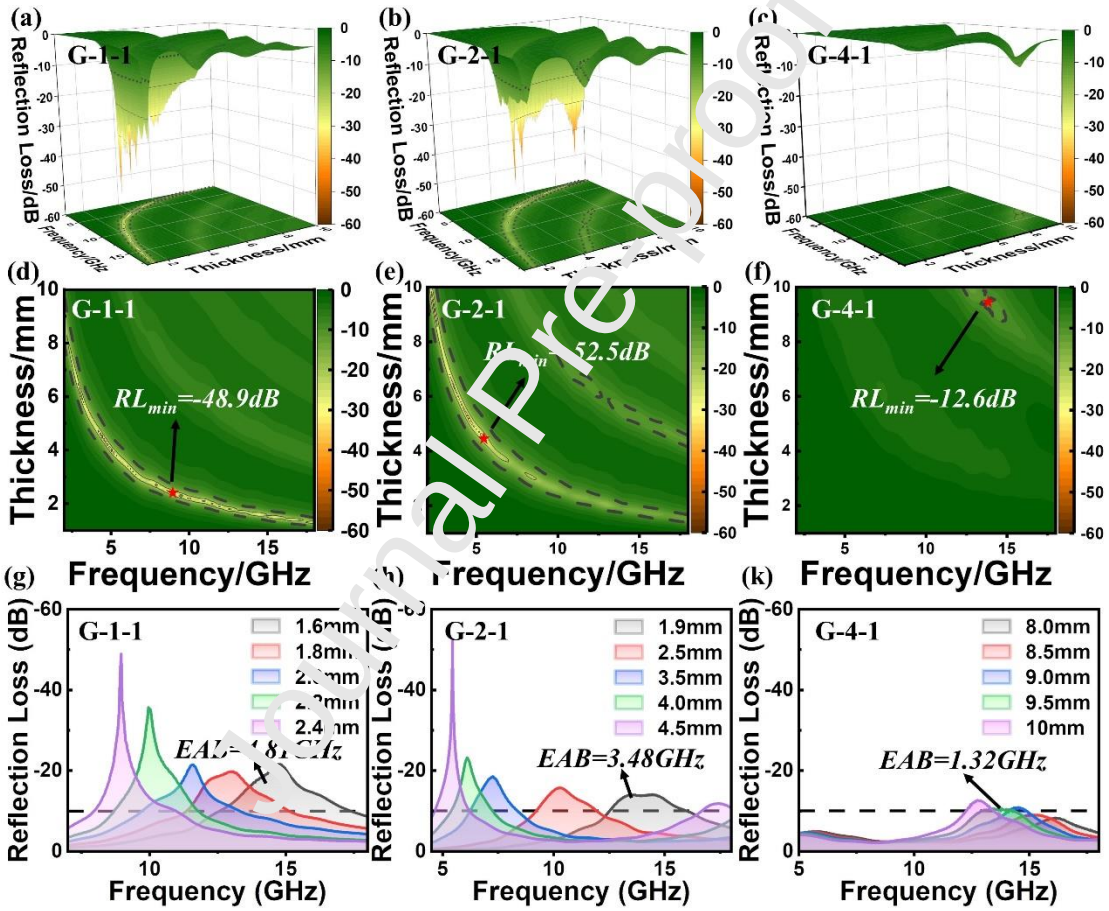

Fig.3 The EMW absorption performance of G-1-1, G-2-1, and G-4-1. (a-c) 3D graphs. (d-f) 2D graphs. (g-k) The reflection loss curves at different thicknesses.

Electromagnetic parameters mainly determine the EMW absorption performance. Thus, complex permittivity is analysed to explain the EMW loss mechanism. The ε' and ε'' represent the storage ability and consumption ability of electromagnetic

energy. As shown in Fig.4 a, the ε' values of all samples decrease gradually with the increase in frequency, which can lead to a widened frequency bandwidth. Furthermore, the more pronounced the change, the wider the absorption bandwidth is [33]. The results show that the slope of G-1-1 is the largest from 18 decreases to 10.5, while the slope of G-4-1 is the least from 4 to 3. Thus, the effective bandwidth of G-1-1 is the broadest, which benefits from the SF and defects of the fluffy spherical structure. Meanwhile, the ε' value of G-1-1 is the highest, which suggests an enormous electric-storage ability. The ε'' value of each sample shows the same trend as seen in Fig.4 (b), and the value decreases from 6.7 to 0.9 as the weight ratio changes from 1:1 to 4:1. The higher ε'' value means the strength dielectric loss ability, which is due to the boosted polarisation relaxation and conductive loss. As observed in Fig.4 (c), the $tan\delta_\varepsilon$ ($\varepsilon''/\varepsilon'$) value of G-1-1 is higher than the others means the balanced storge and loss ability. Furthermore, the polarisation relaxation peaks of ε'' curves can be clearly observed. Based on Debye's theory, the Cole-Cole semicircle (ε''- ε') indicates a corresponding Debye relaxation process, and one semicircle represents one polarisation process. Meanwhile, the bigger the radius, the more powerful the polarisation loss will be [4, 33]. The correlativity between ε' and ε'' value can be obtained through the following Equation:

$$[\varepsilon' - (\varepsilon_s + \varepsilon_\infty)/2]^2 + (\varepsilon'')^2 = [(\varepsilon_s - \varepsilon_\infty)/2]^2 \quad (7)$$

where ε_s is the static permittivity, ε_∞ is the relative permittivity. The polarization relaxation processes are intuitively shown in Fig.4 (e-g). The Cole-Cole curve of G-1-1 has four larger semicircles, while G-4-1 shows the least, indicating that G-1-1 has higher polarisation relaxation loss. The higher property of G-1-1 is due to the SF and defects of fluffy spherical SiC, which can cause a lot of defect-induced polarisation. Meanwhile, the matching value of ε', ε'' and d/λ_0 can be calculated through the

following Equation [34]:

$$tan\,h\left[j(2\pi d\,/\,\lambda_0)\sqrt{\varepsilon'-\varepsilon''}\right]=\sqrt{\varepsilon'-\varepsilon''} \quad (8)$$

where λ_0 is the wavelength of EMW in free space. In theory, if the ε'- ε'' (Cole-Cole) curves of an absorber is closer to the matching curve, the better the input impedance approaching the impedance of free space. The matching line and Cole-Cole curves are shown in Fig.S4. The Cole-Cole curve of G-1-1 is closest to the matching line, which has the best impedance matching condition, resulting in more incident EMW entering the fluffy spherical absorber.

A large amount of SF and defect structure can be further confirmed by Raman spectra and UV-Vis results, as shown in Fig.4 (d,h). From Raman spectra, the three samples all have a strong peak of around 780 cm^{-1}, corresponding to the Transverse Optical phonon mode (TO, the standard characteristic is 796 cm^{-1}) of SiC [35]. The specific TO value of G-1-1, G-2-1 and G-4-1 were 776 cm^{-1}, 789 cm^{-1}, and 790 cm^{-1}. The three samples had a scattering peak near 930 cm^{-1}, corresponding to Longitudinal Optical phonon mode (LO, the standard characteristic is 972 cm^{-1}) [35]. The LO peak of G-1-1, G-2-1 and G-4-1 were 935 cm^{-1}, 924 cm^{-1}, and 929 cm^{-1}. All three samples were shifted, and the FWHM (full width at high maximum) of the TO peak line was large and asymmetric due to the SF and construction defects in the β-SiC [36]. The higher the SF density, the higher the TO peak shifts to the low frequency. The result shows that G-1-1 has the highest SF and defect density of the three samples. The UV-vis absorption spectra show that the Eg of the three samples were 2.28 eV, 2.68 eV and 2.32 eV, respectively. Among the three samples, G-1-1 has a lower bandgap from incomplete crystallization caused by a higher diffusion rate [37]. Meanwhile, the lower the band gap, the easier it is for electrons to be stimulated from the valence band to the conduction band and the higher the conductivity, leading to high

conductive loss [38].

Moreover, these Cole-Cole curves have many loops at high frequencies, illustrating that EMW loss is primarily driven by polarisation loss instead of conduction loss. The fitted results of the contribution of polarisation loss (ε_p") and conduction loss (ε_c") are shown in Fig.4 (i-k). The ε_c" value of each sample decreases with the frequency increase, while the ε_p" value increases first and then slightly decreases. The trend aligned well with the Cole-Cole curves, illustrating that the ε_c" contributes significantly at low frequency and ε_p" contributes greatly at high frequency. The curves also reveal that the ε_c" and ε_p" value of G-1-1 is the highest, which means the EMW can be attenuated most on G-1-1. The ε_p" to ε_c" ratio curves are plotted in Fig.4 (k). The results illustrate that G-1-1 has a higher ratio of conduction loss than polarization loss, which coincides with the UV-Vis spectra results (Fig.4 h).

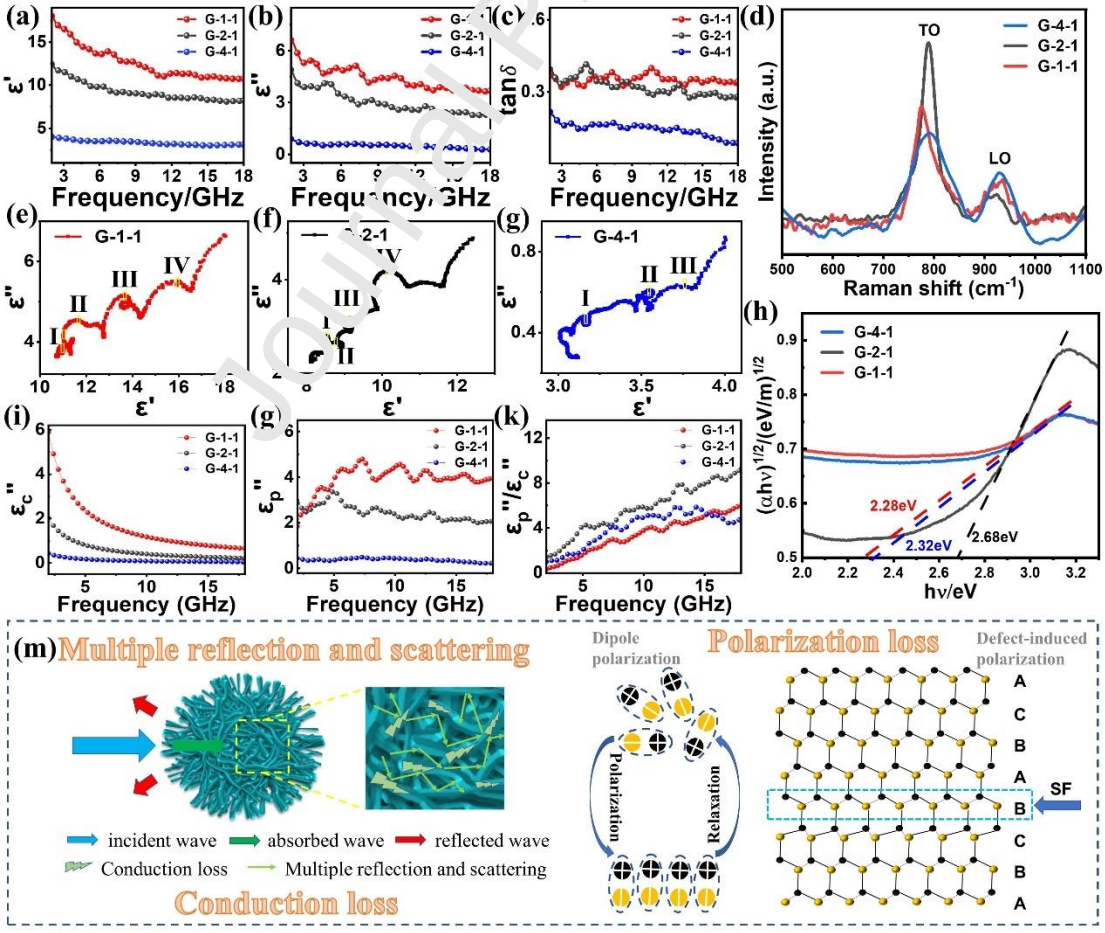

Fig.4 (a) Real permittivity, (b) Imaginary permittivity, (c) Dielectric tangent loss and (d) Raman spectrum of G-1-1, G-2-1, and G-4-1. (e-g) Cole-Cole curves of G-1-1, G-2-1, and G-4-1. (h) Plots of $(ahv)^{1/2}$ versus hv for the indirect transition of G-1-1, G-2-1, G-4-1. Bandgap Eg is obtained by extrapolation to α=0. (i) Conductive loss, (g) Polarisation loss and (k) Ratio of polarisation loss to conductive loss of G-1-1, G-2-1, and G-4-1. (m) Dielectric loss mechanism diagram of G-1-1.

Based on the discussions above, the porous flower-like morphology of G-1-1 exhibits good EMW absorbing properties, and the EMW absorbing mechanism is shown in Fig.4 m. Firstly, the porous soft spherical structure improves the impedance matching condition, giving more EMWs access to the absorber. Meanwhile, the sample has a higher specific surface area (146 $m^2 \cdot g^{-1}$), which means the greater the number of atoms on the surface, leading to polarisation loss. Secondly, the incident EMW is repeatedly reflected and scattered through the porosity of the material, which increases the transmission route of the EMW, making it easier to dissipate EMW energy [39, 40]. Furthermore, the lower band gap of G-1-1 can make the electron transmission easier to generate conduction loss. In addition, the fluffy structure can also form a sizeable conductive network, promoting conductive loss and further attenuating EMW energy. Thirdly, many SF and defects can trap charge carriers to promote defect-induced polarisation and dipole polarisation, leading to more EMW energy converted into heat energy. These multiple synergisms result in an excellent EMW absorption ability of G-1-1. The effective absorption bandwidth of G-1-1 can reach 4.81 GHz at a thickness of only 1.6 mm.

In contrast, the SiC was prepared by commercial silicon under the same ratio and process. Fig. 5 shows that the morphology and EMW absorbing ability of C-1-1, C-2-1, and C-4-1 had the same trend as the products synthesised by glass powder. The comparison of the EMW absorption performance can be clearly seen in Table 1. The EMW absorbing performance is closely related to the morphology of the products,

and the porous fluffy spherical SiC has a better EMW absorption ability than nanofibrous products. In the thickness ranging from 1 mm to 5 mm, the RLmin of G-1-1 and C-1-1 are -48.9 dB and -28.3 dB, and their EAB can reach 4.81 and 4.15 GHz, respectively, indicating that G-1-1 has a better EMW absorbing property than C-1-1. These results also show that glass powder can completely replace commercial silicon to prepare SiC, which realise the reuse of waste glass and saves energy, further protecting the environment.

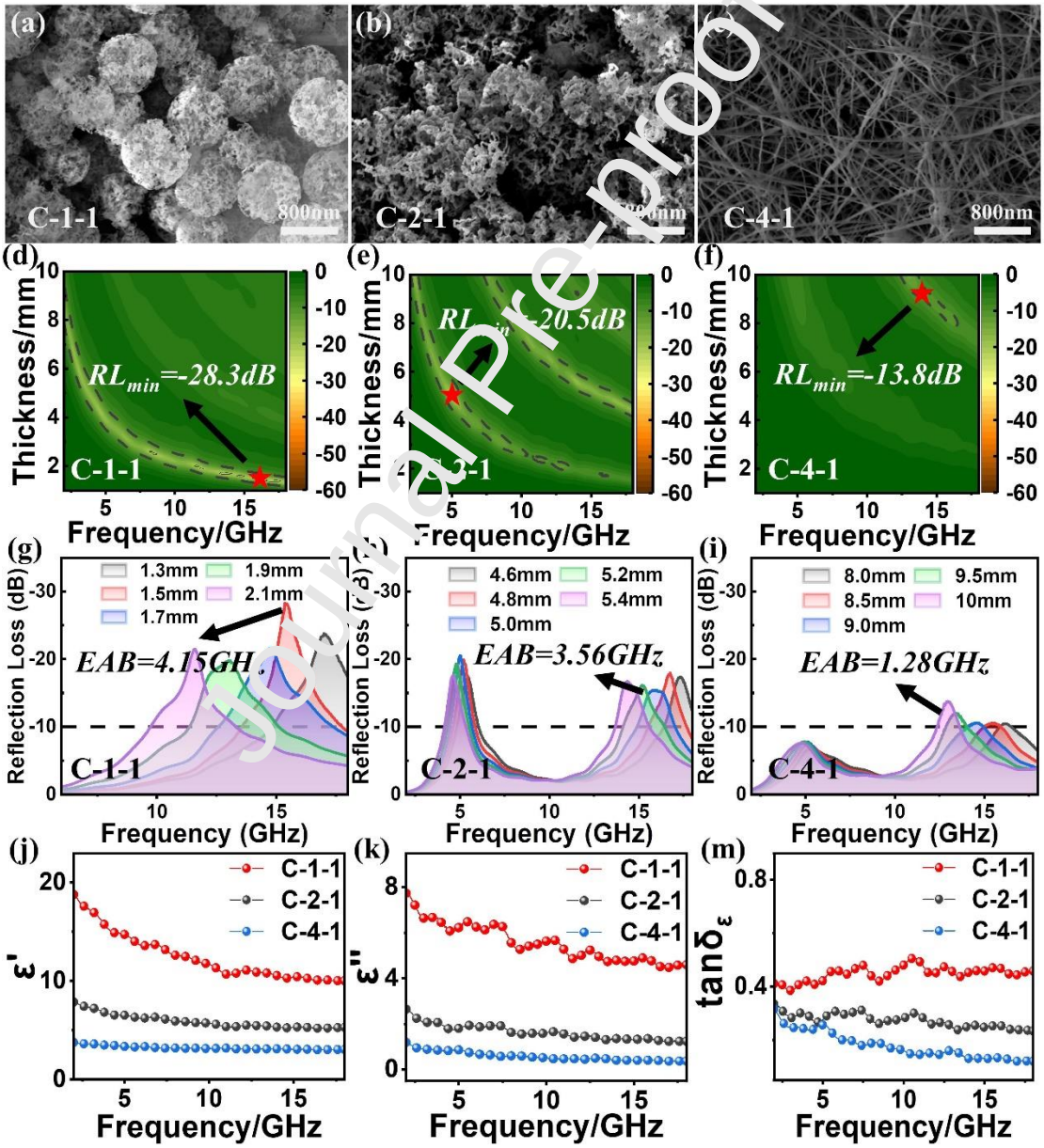

Fig. 5 (a-c) FESEM images of C-1-1, C-2-1, and C-4-1. (d-f) The 2D graphs of EMW absorption

performance of C-1-1, C-2-1, and C-4-1. (g-i) The reflection loss curves at different thicknesses of C-1-1, C-2-1, and C-4-1. (j)Real permittivity, (k) Imaginary permittivity and (m) dielectric loss tangent of C-1-1, C-2-1, and C-4-1.

Table 1 The list of the EMW absorbing performance of each sample.

Samples	Minimum reflection loss(dB)	Effective bandwidth (GHz)	Matching thickness(mm)	Effective bandwidth-(1mm-5mm) (GHz)
G-1-1	-48.9	4.81	1.6	14.60
G-2-1	-52.5	3.48	1.9	13.82
G-4-1	-12.6	1.32	9.5	0.82
C-1-1	-28.3	4.15	1.5	14.60
C-2-1	-20.5	3.56	2	10.28
C-4-1	-13.8	1.28	10	0

The electromagnetic wave absorption performance of some representative morphology of pure SiC is listed in Table 2, which is acquired from some published articles. From the contradistinctive data, porous fluffy flower-like SiC (G-1-1 and C-1-1) shows great EMW absorbing properties. It further proved the significance of preparing SiC with recycled waste glass and broadening its application in the absorber area.

Table 2 A list of electromagnetic wave absorption properties with previously reported pure SiC materials

Samples	Minimum reflection loss(dB)	Effective bandwidth (GHz)	Matching thickness (mm)	Ref.
SiC NWs	-31.7	2.15	2.0	[41]
SiC NWs	-30	3.7	4.6	[42]
Porous SiC	-30	4	4-5	[14]
SiC powders	-22	1.68	1.5	[43]
SiC aerogels	-43	4	2	[15]
Hollow sphere SiC	-51.7	5.82	3.1	[44]
G-1-1	-48.9	4.81	1.6	current work
C-1-1	-28.3	4.15	1.5	current work

4 Conclusions

In this study, the different microstructure of SiC was derived by adequately adjusting the concentration of waste glass, which can evolve from porous fluffy spheres to nanofibers. The competition between the deposition rate and diffusion rate can explain this change. The EMW absorption capacity of each sample was analysed, and the results show that when the ratio of carbon spheres to waste glass powder reaches 1:1, the biggest RL_{min} of SiC (G-1-1) is -48.92 dB at 8.96 GHz. The EAB of G-1-1 is 4.81 GHz at only 1.6 mm. The porous spherical flower-like structure has benefited from the upgraded impedance matching condition, strengthened polarisation loss and conduction loss of the product. The normal SiC prepared through commercial

silicon was compared with SiC synthesised by the waste glass. The test results show that the EMW absorbing property of SiC crafted from waste glass is better, proving that waste glass powder can replace commercial silicon to prepare SiC. This work provides remarkable ideas by expending wasted glass for SiC absorbers towards excellent stability and EMW properties, achieving lower energy expenditure and protecting the environment.

Acknowledgements

This work is supported by the National Natural Science Foundation of China (52172091 and 52172295), Open Fund of Key Laboratory of Materials Preparation and Protection for Harsh Environment (Nanjing University of Aeronautics and Astronautics), Ministry of Industry and Information Technology (56XCA22042).

Declaration of competing interest

The authors declare no conflict of interest.

Data availability

Data will be made available on request.

References

[1] R. Yang, Y. Fan, R. Ye, Y. Tang, X. Cao, Z. Yin, Z. Zeng, MnO2-Based Materials for Environmental Applications, Advanced Materials 33 (2021).
[2] L. Liu, H. Deng, X. Tang, Y. Lu, J. Zhou, X. Wang, Y. Zhao, B. Huang, Y. Shi, Specific electromagnetic radiation in the wireless signal range increases wakefulness in mice, Proceedings of the National Academy of Sciences of the United States of America 118 (2021) e2105838118.
[3] PiyushP.Gandhi, NaliniR.Humaney, Effects of static electromagnetic fields on sleep patterns: a cross-sectional study, International Journal of Research in Medical Sciences 8 (2020) 1853-1859.
[4] J.Q. Tao, J.T. Zhou, Z.J. Yao, Z.B. Jiao, B. Wei, R.Y. Tan, Z. Li, Multi-shell hollow porous carbon nanoparticles with excellent microwave absorption properties, Carbon 172 (2021) 542-555.
[5] J.Q. Tao, L.L. Xu, L. Wan, J.S. Hou, P.S. Yi, P. Chen, J.T. Zhou, Z.J. Yao, Cubic-like Co/NC composites derived from ZIF-67 with a dual control strategy of size and graphitization degree for microwave absorption, Nanoscale 13 (2021) 12896-12909.
[6] J.T. Zhou, B. Wei, M.Q. Wang, Z.J. Yao, P. Chen, C.Y. Zhou, Z.J. Li, Three dimensional flower like ZnFe2O4 ferrite loaded graphene: Enhancing microwave absorption performance by constructing microcircuits, Journal of Alloys and Compounds 889 (2021).
[7] S. Li, X. Tang, X. Zhao, S. Lu, J. Luo, Z. Chai, T. Ma, Q. Lan, P. Ma, W. Dong, Z. Wang, T. Liu, Hierarchical graphene@MXene composite foam modified with flower-shaped FeS for efficient and broadband electromagnetic absorption, Journal of Materials Science & Technology 133 (2023) 238-248.
[8] S. Zhong, M. Yu, X. Liang, Y. Dong, J. Liu, C. Wang, Microwave absorption performance and multiple loss mechanisms of three-dimensional porous Fe4N@Fe3O4@Fe/carbon composite, Journal of Materials Science 57 (2022) 16649-16664.
[9] X. Yin, L. Kong, L. Zhang, L. Cheng, N. Travitzky, P. Greil, Electromagnetic properties of Si–C–N based ceramics and composites, International Materials Reviews 59 (2014) 326-355.
[10] P. Melinon, B. Masenelli, F. Tournus, A. Perez, Playing with carbon and silicon at the nanoscale, Nature Materials 6 (2007) 479-490.
[11] J. Liu, X. Wei, L. Gao, J. Tao, L. Xu, G. Peng, H. Jin, Y. Wang, Z. Yao, J. Zhou, An overview of C-SiC microwave absorption composites serving in harsh environments, Journal of the European Ceramic Society 43 (2023) 1237-1254.
[12] Z. Wu, C. Yao, Z. Meng, H. Zheng, H. Zhou, X. Yang, Y. Li, Enhancement of the electromagnetic wave absorption via the bamboo-like SiC whiskers with high-density stacking faults, Journal of Materials Science-Materials in Electronics 33 (2022) 21351-21362.
[13] T. Xiao, J. Kuang, H. Pu, Q. Zheng, Y. Lu, W. Liu, W. Cao, Hollow SiC microtube with multiple attenuation mechanisms for broadband electromagnetic wave absorption, Journal of Alloys and Compounds 862 (2021) 158032.
[14] C. Liu, D. Yu, D.W. Kirk, Y. Xu, Porous silicon carbide derived from apple fruit with high electromagnetic absorption performance, Journal of Materials Chemistry C 4 (2016) 5349-5356.
[15] C. Liang, Z. Wang, Eggplant-derived SiC aerogels with high-performance electromagnetic wave absorption and thermal insulation properties, Chemical Engineering Journal 373 (2019) 598-605.

[16] J. Liu, J. Tao, L. Gao, X. He, B. Wei, Y. Gu, Z. Yao, J. Zhou, Morphology-size synergy strategy of SiC@C nanoparticles towards lightweight and efficient microwave absorption, Chemical Engineering Journal 433 (2022) 134484.
[17] Y. Xia, K.D. Gilroy, H.C. Peng, X. Xia, Seed-Mediated Growth of Colloidal Metal Nanocrystals, Angew Chem Int Ed Engl 56 (2017) 60-95.
[18] R. Tan, J. Zhou, Z. Yao, B. Wei, J. Zu, H. Lin, Z. Li, Ferrero Rocher® chocolates-like FeCo/C microspheres with adjustable electromagnetic properties for effective microwave absorption, Journal of Alloys and Compounds 857 (2021).
[19] X. Xia, J. Zeng, L.K. Oetjen, Q. Li, Y. Xia, Quantitative analysis of the role played by poly(vinylpyrrolidone) in seed-mediated growth of Ag nanocrystals, J Am Chem Soc 134 (2012) 1793-1801.
[20] C. Liang, Z. Wang, L. Wu, X. Zhang, H. Wang, Z. Wang, Light and Strong Hierarchical Porous SiC Foam for Efficient Electromagnetic Interference Shielding and Thermal Insulation at Elevated Temperatures, ACS Appl Mater Interfaces 9 (2017) 29950-29957.
[21] M.E. Bathen, C.T.K. Lew, J. Woerle, C. Dorfer, U. Grossner, S. Castelletto, B.C. Johnson, Characterization methods for defects and devices in silicon carbide, Journal of Applied Physics 131 (2022).
[22] V. Jabbari, J.M. Veleta, M. Zarei-Chaleshtori, J. Gardea-Torresdey, D. Villagrán, Green synthesis of magnetic MOF@GO and MOF@CNT hybrid nanocomposites with high adsorption capacity towards organic pollutants, Chemical Engineering Journal 304 (2016) 774-783.
[23] W.H. Huang, Q. Qiu, X.F. Yang, S.W. Xue, J.A. Bai, H.B. Zhang, K. Pei, R.C. Che, Ultrahigh Density of Atomic Co-Fe-Electron Synergy in Noncontinuous Carbon Matrix for Highly Efficient Magnetic Wave Adsorption, Nano-Micro Letters 14 (2022).
[24] X.X. He, J.T. Zhou, J.Q. Tao, Y.J. Liu, B. Wei, Z.J. Yao, X.W. Tao, Preparation of porous CoNi/N-doped carbon microspheres based on magnetoelectric coupling strategy: A new choice against electromagnetic pollution, Journal of Colloid and Interface Science 626 (2022) 123-135.
[25] J. Tao, J. Zhou, Z. Yao, Z. Jiao, B. Wei, R. Tan, Z. Li, Multi-shell hollow porous carbon nanoparticles with excellent microwave absorption properties, Carbon 172 (2021) 542-555.
[26] L. Yan, C. Hong, B. Sun, G. Zhao, Y. Cheng, S. Dong, D. Zhang, X. Zhang, In Situ Growth of Core-Sheath Heterostructural SiC Nanowire Arrays on Carbon Fibers and Enhanced Electromagnetic Wave Absorption Performance, ACS Appl Mater Interfaces 9 (2017) 6320-6331.
[27] L. Wang, X. Li, X. Shi, M. Huang, X. Li, Q. Zeng, R. Che, Recent progress of microwave absorption microspheres by magnetic-dielectric synergy, Nanoscale 13 (2021) 2136-2156.
[28] C. Liu, D. Yu, Donald W. Kirk, Y. Xu, Electromagnetic wave absorption of silicon carbide based materials, RSC Advances 7 (2017) 595-605.
[29] L.L. Xu, J.Q. Tao, X.F. Zhang, Z.J. Yao, A. Zavabeti, J.T. Zhou, Co@N-doped double-shell hollow carbon via self-templating-polymerization strategy for microwave absorption, Carbon 188 (2022) 34-44.
[30] B. Wei, C.Y. Zhou, Z.J. Yao, L.L. Xu, Z.J. Li, L. Wan, J.S. Hou, J.T. Zhou, Lightweight and high-efficiency microwave absorption of reduced graphene oxide loaded with irregular magnetic quantum dots, Journal of Alloys and Compounds 886 (2021).
[31] J.Q. Tao, Z.B. Jiao, L.L. Xu, P.S. Yi, Z.J. Yao, F. Yang, C.Y. Zhou, P. Chen, J.T.

Zhou, Z. Li, Construction of MOF-Derived Co/C shell on carbon fiber surface to enhance multi-polarization effect towards efficient broadband electromagnetic wave absorption, Carbon 184 (2021) 571-582.
[32] J.T. Zhou, J.Q. Tao, Z.J. Yao, L.L. Xu, Z. Li, P. Chen, Ag Nanoparticles Embedded in Multishell Carbon Nanoparticles for Microwave Absorption, Acs Applied Nano Materials 4 (2021) 5425-5436.
[33] Z.B. Jiao, W.J. Huyan, J.R. Yao, Z.J. Yao, J.T. Zhou, P.J. Liu, Heterogeneous ZnO@CF structures and their excellent microwave absorbing properties with thin thickness and low filling, Journal of Materials Science & Technology 113 (2022) 166-174.
[34] J. Wang, J. Zhou, H. Van Zalinge, Z. Yao, L. Yang, Hollow SiC@MnO2 nanospheres with tunable core size and shell thickness for excellent electromagnetic wave absorption, Chemical Engineering Journal 471 (2023).
[35] G. Cambaz, G. Yushin, Y. Gogotsi, V. Lutsenko, Anisotropic etching of SiC whiskers, Nano Lett 6 (2006) 548-551.
[36] S. Rohmfeld, M. Hundhausen, L. Ley, Influence of stacking disorder on the Raman spectrum of 3C-SiC, PHYSICA STATUS SOLIDI B-BASIC RESEARCH 215 (1999) 115-119.
[37] K. Reddy, S. Manorama, A. Reddy, Bandgap studies on anatase titanium dioxide nanoparticles, Materials Chemistry and Physics 78 (2003) 239-245.
[38] J. Chen, G. Yang, R. Wu, Y. Pan, J. Lin, R. Zhai, L. Wu, Large-scale synthesis and characterization of hexagonal prism-shaped SiC nanowires, J Nanosci Nanotechnol 8 (2008) 2151-2156.
[39] F. Mao, X. Fan, L. Long, Y. Li, H. Chen, W. Zhou, Constructing 3D hierarchical CNTs/VO2 composite microspheres with superior electromagnetic absorption performance, Ceramics International 49 (2023) 16924-16931.
[40] W. Zhou, Y. Zhang, Y. Li, Y. Gou, X. Zhou, In-situ synthesis of ternary layered Y3Si2C2 ceramic on silicon carbide fiber for enhanced electromagnetic wave absorption, Ceramics International 48 (2022) 1908-1915.
[41] S.-C. Chiu, H.-C. Yu, Y.-Y. Li, High Electromagnetic Wave Absorption Performance of Silicon Carbide Nanowires in the Gigahertz Range, Journal of Physical Chemistry C 114 (2010) 1947-1952.
[42] H. Zhang, Y. Xu, J. Zhou, J. Jiao, Y. Chen, H. Wang, C. Liu, Z. Jiang, Z. Wang, Stacking fault and unoccupied densities of state dependence of electromagnetic wave absorption in SiC nanowires, Journal of Materials Chemistry C 3 (2015) 4416-4423.
[43] Y. Wang, P. Xiao, W. Zhou, H. Luo, Z. Li, W. Chen, Y. Li, Microstructures, dielectric response and microwave absorption properties of polycarbosilane derived SiC powders, Ceramics International 44 (2018) 3606-3613.
[44] J. Zhou, B. Wei, Z. Yao, H. Lin, R. Tan, W. Chen, X. Guo, Preparation of hollow SiC spheres with biological template and research on its wave absorption properties, Journal of Alloys and Compounds 819 (2020) 153021.

Conflict of interest

The authors declared that they have no conflicts of interest in this work.

Declaration of interests

☒ The authors declare that they have no known competing financial interests or personal relationships that could have appeared to influence the work reported in this paper.

☐The authors declare the following financial interests/personal relationships which may be considered as potential competing interests:

1. Successfully prepared different morphological SiC absorbers.

2. The competition between diffusion and deposition rates leads to a change in morphology.

3. The effective absorption bandwidth of the porous fluffy spherical SiC can reach 4.81 GHz at 1.6 mm.